Low-frequency, high-density, inductively coupled plasma sources: Operation and applications

S. Xu, K. N. Ostrikov, Y. Li, E. L. Tsakadze, and I. R. Jones

Citation: Physics of Plasmas (1994-present) **8**, 2549 (2001); doi: 10.1063/1.1343887
View online: http://dx.doi.org/10.1063/1.1343887
View Table of Contents: http://scitation.aip.org/content/aip/journal/pop/8/5?ver=pdfcov
Published by the AIP Publishing

Low-frequency, high-density, inductively coupled plasma sources: Operation and applications*

S. Xu[†,a)]
Plasma Processing Laboratory, NIE, Nanyang Technological University, 1 Nanyang Walk, 637616 Singapore

K. N. Ostrikov[b)]
Plasma Processing Laboratory, NIE, Nanyang Technological University, 1 Nanyang Walk, 637616 Singapore, Department of Physics, Flinders University of South Australia, GPO Box 2100, Adelaide SA 5001, Australia, and Department of Electrical Engineering, Nagoya University, Nagoya 464-8603, Japan

Y. Li and E. L. Tsakadze
Plasma Processing Laboratory, NIE, Nanyang Technological University, 1 Nanyang Walk, 637616 Singapore

I. R. Jones
Department of Physics, Flinders University of South Australia, GPO Box 2100, Adelaide SA 5001, Australia

(Received 25 October 2000; accepted 6 November 2000)

Operation regimes, plasma parameters, and applications of the low-frequency (~500 kHz) inductively coupled plasma (ICP) sources with a planar external coil are investigated. It is shown that highly uniform, high-density ($n_e \sim 9\times10^{12}$ cm^{-3}) plasmas can be produced in low-pressure argon discharges with moderate rf powers. The low-frequency ICP sources operate in either electrostatic (E) or electromagnetic (H) regimes in a wide pressure range without any Faraday shield or an external multipolar magnetic confinement, and exhibit high power transfer efficiency, and low circuit loss. In the H mode, the ICP features high level of uniformity over large processing areas and volumes, low electron temperatures, and plasma potentials. The low-density, highly uniform over the cross-section, plasmas with high electron temperatures and plasma and sheath potentials are characteristic to the electrostatic regime. Both operation regimes offer great potential for various plasma processing applications. As examples, the efficiency of the low-frequency ICP for steel nitriding and plasma-enhanced chemical vapor deposition of hydrogenated diamond-like carbon (DLC) films, is demonstrated. It appears possible to achieve very high nitriding rates and dramatically increase micro-hardness and wear resistance of the AISI 304 stainless steel. It is also shown that the deposition rates and mechanical properties of the DLC films can be efficiently controlled by selecting the discharge operating regime.
[DOI: 10.1063/1.1343887]

I. INTRODUCTION

Recently, there has been an increasing interest in high-density low-temperature plasmas for material processing applications, which include the fabrication of microelectronic materials and devices, material surface structuring and modification, thin films deposition and etching, and plasma-assisted synthesis of novel materials.[1,2] High uniformity of ions and active species, high product yield with low damage, process selectivity, and reproducibility are the common requirements for plasma processing.[3] The sources of inductively coupled plasmas (ICPs) with an external planar coil have proven to meet the above requirements.[4] The flat spiral coil is powered by a rf generator through a matching circuit. Typically, the 13.56 MHz rf is used to drive the induced currents and sustain the discharge maintaining the ionization of neural gas at a required level, although several works reported discharge operation at different frequencies, ranging from low[5] to ultra-high frequencies.[6]

To date, a substantial amount of theoretical and experimental works on inductively coupled plasmas has been carried out (see, e.g., Refs. 4, 7 and the references therein). In particular, it has been clearly demonstrated that at low powers, the ICP discharge starts in the low-density electrostatic regime, usually referred to as the E-mode. An increase of the rf power to a certain threshold results in transition to the high-density regime (H-mode). Transitions between the two discharge regimes are accompanied by jumps in plasma and circuit parameters. Furthermore, the E→H and H→E transitions occur under different values of the coil current, and a cyclic variation of the rf input power results in the nonlinear discharge hysteresis.[8–11] The nonlinearity of inductively

*Paper BI2 5, Bull. Am. Phys. Soc. **45**, 20 (2000).
[†]Invited speaker.
[a)]Electronic mail: syxu@nie.edu.sg
[b)]Also at School of Electrical and Electronic Engineering, Nanyang Technological University, Nanyang Avenue, 639798 Singapore.

coupled plasmas is further evidenced by the observation of strong second harmonic rf currents even at low input powers.[12] Physically, higher harmonic signals presumably originate due to the action of the nonlinear Lorentz force on plasma electrons and ions.[7] Above all, the strong ponderomotive forces are expected to come into play and strongly modify the plasma parameters through the generation of steady-state nonlinear electromagnetic fields.[13]

The low-frequency (LF) devices have recently become very attractive as efficient sources of industrial plasmas. As has been evidenced by previous works,[5,8,14–17] the LF ICPs possess a number of indisputable advantages that make them especially useful as prototypes of commercial large-area plasma reactors. In this article, we investigate the key features of inductively coupled plasmas produced in low-frequency ($\sim$500 KHz) plasma sources at Nanyang Technological University, Singapore[15–17] and the Flinders University of South Australia.[8,14] The implications and advantages of the low-frequency operation regime are emphasized. We also confirm that the LF ICPs feature nonlinear hysteresis and higher harmonic generation effects. Furthermore, as the intensity of nonlinear plasma responses[18] usually declines with operating frequency, we can expect that the nonlinear hysteresis and higher harmonic generation effects will be stronger than in conventional 13.56 MHz plasma sources. Likewise, we demonstrate the application of the LF ICP source for the plasma-enhanced nitrogen ion implantation and diffusion into the stainless steel and chemical vapor deposition (CVD) of hydrogenated diamond-like-carbon (DLC) films.

The paper is organized as follows. In Sec. II, we describe the experimental set-up, ancillary equipment, and diagnostic tools. Discharge operation and uniformity of plasma parameters are studied in Sec. III. Section IV is devoted to the E↔H mode transitions and discharge hysteresis and analysis of the behavior of the plasma parameters, optical emission intensity, and electromagnetic fields during the mode transitions. In Sec. V, the application of the LF ICP source for rapid steel nitriding and plasma enhanced chemical vapor deposition (PECVD) synthesis of diamond-like-carbon films is demonstrated. The key features of the plasma source and the implications of the low-frequency operation are discussed in Sec. VI. We end the paper with Conclusions where the results obtained are summarized.

II. THE LF ICP SOURCE AND DIAGNOSTICS

The experiments were carried out at the Nanyang Technological University (NTU), Singapore, and the Flinders University of South Australia on two similar plasma sources. Here we mainly concentrate on the results obtained at NTU, and, where applicable, refer the reader to earlier works done at Flinders University.

A. The LF ICP source

A schematic diagram of the experimental set-up is sketched in Fig. 1 (note the coordinates used in this work). The plasma is generated in a cylindrical, stainless steel walled vacuum chamber with the inner diameter $2R=32$ cm and length $L=20$ cm. The chamber is cooled by continuous water flow in between the inner and outer walls of the chamber. Four rectangular side ports and 15 radially aligned holes in the bottom allow the access for various diagnostic tools. The top plate of the chamber is a fused silica disk, 35 cm diameter and 1.2 cm thick, which forms a vacuum-tight dielectric window. The chamber is evacuated by a 450 $\mathrm{l\,s^{-1}}$ turbo-molecular pump backed by a two-stage rotary pump. The typical base pressure of $\sim 2\times10^{-5}$ Torr is routinely achieved. The inflow rate and pressure of the working gas are regulated by a combination of a gate valve and MKS mass-flow controllers. The pressure is measured by MKS Baratron capacitance manometer. The operating pressure is typically maintained in the range $p_0=0.3$–1000 mTorr, important for most plasma processing applications.[3]

The rf field is generated by means of a 17 turn, flat spiral coil made of 6.35 mm diameter copper tube (with the cooling water flows inside) firmly fixed 3 mm above the quartz window atop of the vacuum chamber. A low frequency (500 kHz) rf generator is used to drive the flat spiral coil through a matching network.

The rf generator is connected to the rf coil via a matching network. The equivalent circuit of the LF ICP source is given in Fig. 1(b). Here V_0 and R_0 are the open circuit voltage and resistance of the rf generator, V_i and I_i are the input voltage and current into the matching network, R_c and L_c are the resistance and inductance of the unloaded coil, ΔL_p is the variable part of the circuit inductance due to the plasma load, R_p is a reflected plasma resistance, I_c is the coil current, and $L=L_c-\Delta L_p$. Capacitors C_1 and C_2 are used to match the rf generator to the plasma load. In calculating the power deposited in the plasma, the power dissipated in the coil has been deducted straightforwardly. We note that $X=(V_i/I_c)\sin\phi=\omega L-(1/\omega C_1)=X_c-\Delta X_p$ is the total circuit reactance, X_c and ΔX_p are the unloaded circuit reactance and a reactance change due to the plasma, and ϕ is the phase shift between V_i and I_c, respectively.[14,17]

B. Plasma diagnostics

The rf voltage V_i and the circuit currents I_i, I_c are measured using Tektronix P6009 voltage probes and the two Pearson current transducers (model 1025), respectively. The rf signals are digitized by the Tektronik TDS 460 digital storage oscilloscopes before being transferred to a computer for analysis.

The rf magnetic fields are measured using two miniature magnetic probes each consisting of 12 turn windings on the end of 5 mm diameter fused silica tube. One of them senses the radial component whereas the other senses both axial and azimuthally components, with appropriate orientation. The probe is inserted either horizontally or vertically through the holes in the side port or bottom of the chamber.

The electron density, temperature, and plasma potential have been measured using a rf compensated single cylindrical Langmuir probe. The probe can be moved radially and

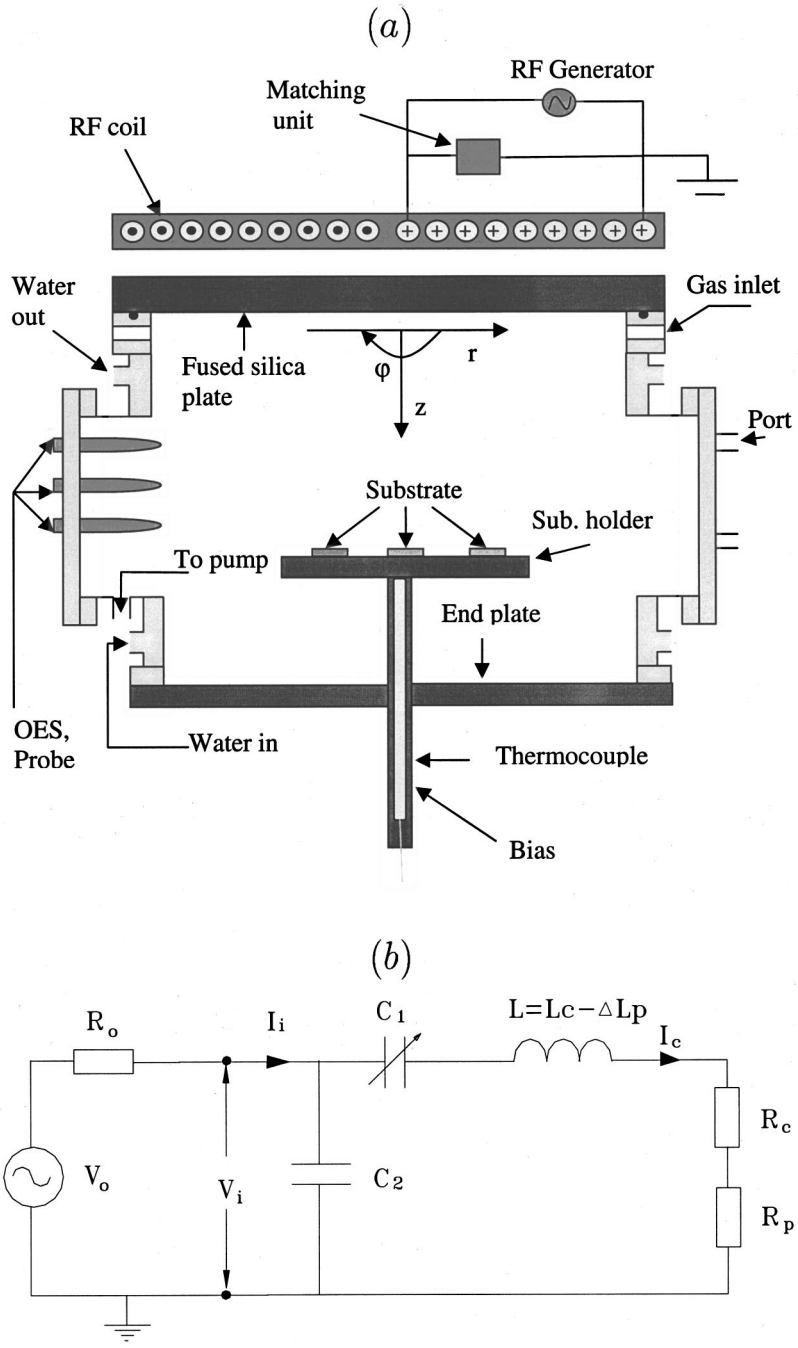

FIG. 1. Sketch (a) and equivalent circuit diagram (b) of the LF ICP source.

axially through one of the four port windows or holes in the bottom plate. The Langmuir probe data on both set-ups are cross-referenced by the integrated electron density provided by the heterodyne microwave interferometer at Flinders University.[19]

The optical emission from the ICP discharge has been collected using a light receiver mounted on the side facing view-port and transmitted via the optical fiber to SpectroPro-750 monochromator/spectrometer. The latter provided resolution of 0.023 nm scanning over the wavelength spectrum from 350 to 850 nm. Other details about the experimental set-ups and plasma diagnostic can be found elsewhere.[8,14,15,17]

III. SOURCE OPERATION AND PLASMA PARAMETERS

In this section, we describe the operation of the plasma source and give insight into measurements of electromagnetic properties of the discharge. Radial and axial profiles of the plasma potential, electron density, and temperature are studied. We also demonstrate that the plasma source can efficiently operate in a wide range of the filling gas pressures.

A. Electromagnetic properties

The source performance experiments have been conducted in argon gas in the pressure range of 0.3–1000

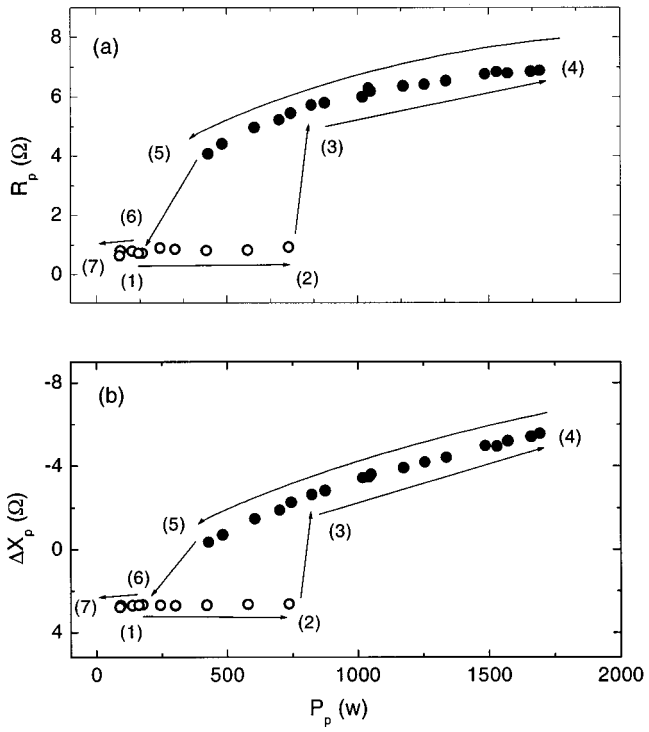

FIG. 2. Reflected plasma resistance (a) and change in load reactance (b) *versus* power absorbed by the plasma for $p_0 = 12$ mTorr.

mTorr.[14,17] Prior to the discharge, the chamber was filled with argon at the pre-determined pressure. The matching/tuning capacitors and the generator bank voltage were set to initial levels. The rf generator has then been turned on. It is noteworthy that, to avoid damage of generator by strong rf currents reflected by poorly matched circuits, the discharge was always started with low rf powers, and the matching has been adjusted properly thereafter. Thus, the discharge always started in a faint electrostatic (E) mode sustained by the potential drop between the inner and outer rf coils.[8,14] A gradual increase of the rf generator output results in discharge transition to a high-density and visually much brighter regime (H-mode). Thereafter, the power input has been slowly decreased back to the minimum starting level. The peak-to-peak voltage, coil current and the phase difference between them have been continuously recorded.

Figure 2 displays the plasma load resistance R_p and reactance change ΔX_p as a function of the power dissipated in the plasma P_p in 12 mTorr Ar discharge. The process starts at point (1) corresponding to a faint E-mode, the discharge remains faint until reaching the state (2). The subsequent increase of the power P_p leads to a sudden transition to a bright H-mode point (3). It is clearly seen from Fig. 2 that the E→H transition is accompanied by a substantial raise of the amount of the plasma resistance R_p and a significant decrease of the coil current I_c and the plasma reactance ΔX_p. Thereafter, the input power has been continuously increased, and the discharge remains in the H-mode. As the rf power is increased further, the value of ΔX_p further decreases, while the plasma resistance R_p steadily grows (Fig. 2).

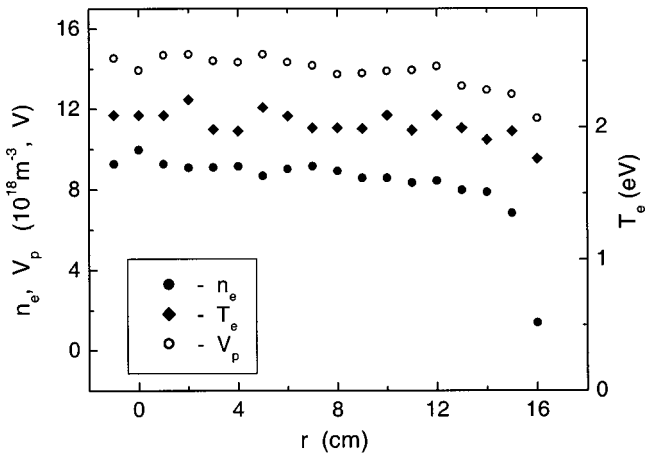

FIG. 3. Radial profiles of the electron density n_e, temperature T_e, and plasma potential V_p in a 22 mTorr, H-mode Ar discharge. The rf input power is 1.7 kW.

After reaching the state (4), where the P_p is maximal, the coil current has been lowered and the discharge still remains in the H-mode even after passing point (3) of the original E→H transition. The inverse H→E transition occurs at coil current I_c [point (5)] less than that of E→H transition. Point (6) corresponds to the E-mode discharge phase. Discharge end at point (7). We note that the discharge is bistable if 220 W $< P_p <$ 840 W. In this case the two different values of circuit parameters correspond to the same rf power. The observed process is cyclic and highly reproducible.

The global electric quantities R_p and ΔX_p can be used to obtain the spatially averaged plasma parameters. Using a simple transformer model, El-Fayoumi and Jones[14] interpreted their electrical measurements by considering the rf coil to form the primary, and the plasma to act as a single-turn secondary coil, of an air-core transformer. The measured circuit quantities are then linked to the electromagnetic fields through the power balance equation. This model provides an efficient and simple way in design of the rf coupling circuit and in understanding of the general properties of LF ICP discharges. For further details, we refer the reader to Refs. 8 and 14.

B. Plasma parameters

The detailed Langmuir probe scans have been performed inside the chamber, and the spatial profiles of electron density n_e, temperature T_e, and plasma potential V_p have been obtained for various total input power and filling pressure. The axial profiles of the plasma parameters have been measured at 7 available axial positions in the side-ports. The radial distributions are obtained by moving the probe along the diameter of the chamber at the central port ($z = 10$ cm) position.

Figure 3 shows the radial profiles of n_e, T_e, and V_p for total input power $P_{\text{tot}} \sim 1.7$ kW in a 22 mTorr, H-mode argon discharge. These profiles reveal that a high density, highly uniform plasma is produced throughout the entire cross-

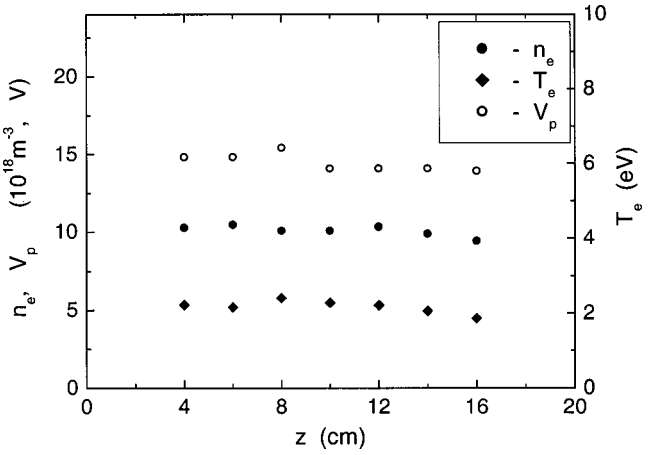

FIG. 4. The same as in Fig. 3, axial profiles.

section of the discharge chamber. The radial nonuniformity of the electron density is estimated to be less than 8% over the radii of the chamber $R<15$ cm. The value of the electron number density is very high ($n_e \sim 9\times10^{12}$ cm^{-3}). The plasma potential (13–17 V) is quite low; so is the electron temperature ($\sim$2.5 eV).

The axial profiles of n_e, T_e, and V_p measured at $r=0$ for the same discharges are displayed in Fig. 4. It is seen that the electron density, temperature, and plasma potential gradually decrease along the axial direction. This result agrees with the Chakrabarty's heterodyne microwave interferometer measurements.[19]

Another important feature of the LF ICP discharge is that it can be operated in a broad range of the filling gas pressures. Figure 5 depicts how the electron density, temperature, and plasma potential vary with the argon gas pressure. It is seen that n_e increases with pressure if $p_0<200$ mTorr and declines in the succeeding range. The electron temperature and plasma potential also diminish with increasing the filling gas pressure. It is worth emphasizing that the source operation is highly reproducible in a broad gas pressure range (0.3–900 mTorr).

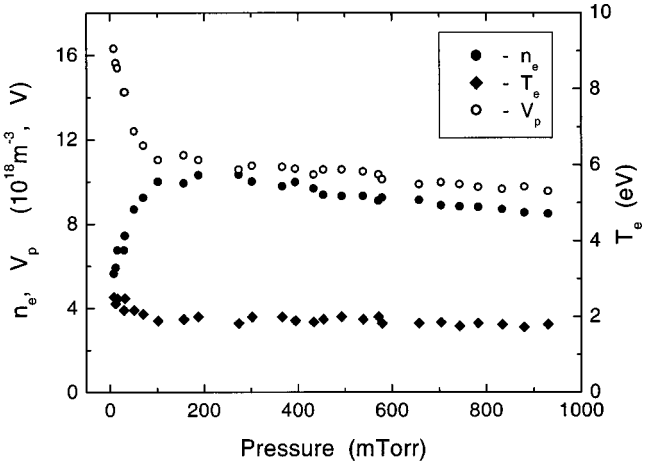

FIG. 5. Electron density, electron temperature, and plasma potential *versus* argon pressure for $P_{tot}=1700$ W, measured at the chamber center.

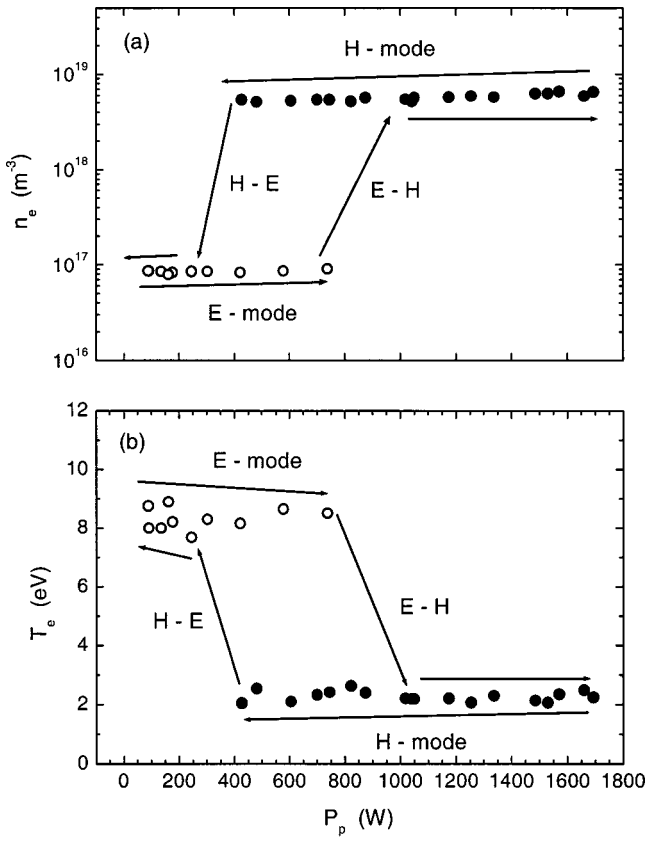

FIG. 6. The changes of n_e (a) and T_e (b) in the course of E↔H transitions. Parameters are the same as in Fig. 3.

IV. DISCHARGE HYSTERESIS

As was mentioned above, the cyclic variation of the input power results in strongly nonlinear hysteresis of the circuit parameters. Here, we reveal that hysteresis is also the case for the plasma parameters and the optical emission intensities. It will also be shown that the E→H transition is accompanied by the generation of strongly nonlinear electromagnetic fields.

A. Variation of plasma parameters

The important feature of the LF ICP is a discontinuous transition of the plasma parameters during the E↔H mode transitions. Figure 6 reveals that in the 22 mTorr discharge, the electron density instantaneously increased by about two orders of magnitude from $n_e \sim 6\times10^{10}$ cm^{-3} to $n_e \sim 8\times10^{12}$ cm^{-3} in the vicinity of E→H transition. The inverse H→E transition, which occurs if the input power diminishes to $\sim$400 W, is accompanied by a sharp down-jump of n_e. Within the H-mode discharge, the electron temperature remains almost constant ($T_e \sim 2.5$ eV) and is not affected by the variation of the input power in the range 400–1700 W. In the E-mode, the average value of T_e ($\sim$8.5 eV) turns out to be higher than in the electromagnetic regime.

B. Optical emission spectra

The optical emission spectra of excited neutral and/or ionized argon atoms have been investigated in the wavelength range 350–850 nm. The plasma species have been

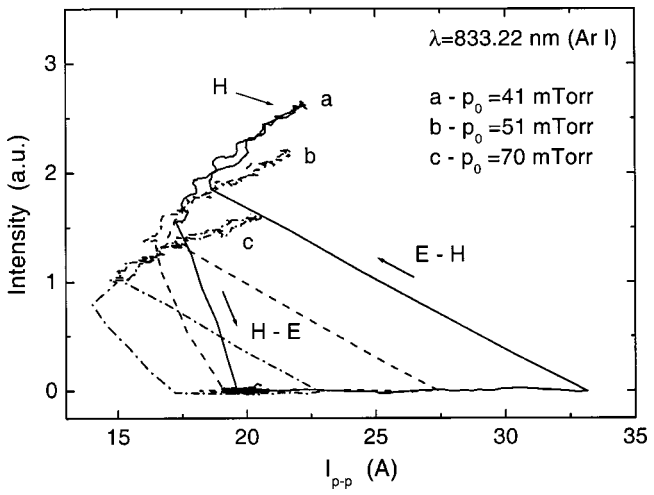

FIG. 7. Variation of the optical emission intensity of Ar^0 line (833.22 nm) during E-↔H-mode transitions.

identified by wavelengths and intensities of their emission lines. The optical emission intensity (OEI) profiles for various species have also been obtained as a function of radial and axial position. It has been observed that the OEI undergoes considerable changes during the E↔H transitions.

The cyclic variation of the OEI corresponding to the 833.22 nm line of a neutral Ar atom with the coil current is depicted in Fig. 7 for different gas pressures. It is clearly seen that the E→H transition is accompanied by an instantaneous raise of the OEI. In the H-mode regime, the OEI further increases with the coil current. A similar tendency has been reported[9] for mode transitions in a helical inductively coupled plasma source. However, the intensity diminishes linearly with reducing the coil current, and the discharge is still in the bright H-mode even for coil currents smaller than the E→H transition current. Near the point of the H→E transition the OEI decreases to the level corresponding to the dim E-mode. In the electrostatic regime, the OEI does not change much and remains low.

Using the OEI data, one can obtain the dependence of the minimal starting current that initiates the E→H transition, and the minimal H-mode maintenance current (threshold current for the H→E transition) on the operating gas pressure.[15] The E→H and H→E transitions are initiated at different values of the gas pressure for the same coil current I_c, which confirms that hysteresis also occurs with variation of the filling gas pressure.

C. Nonlinear electromagnetic fields

To demonstrate that the nonlinear effects are important in the low-frequency ICPs, the components of the rf magnetic field B have been measured in both discharge regimes. Figure 8 shows the radial profiles of the amplitudes of the fundamental and second harmonics of the field measured at $z=4$ cm. It is seen that in the low power, E-mode discharge, only fundamental harmonics of the magnetic fields are present.

After transition to the electromagnetic mode, the magnetic fields change dramatically. The fundamental harmonics of B_z and B_r components diminish compared to their values in the E-mode (note $P_p \sim 230$ W in the E-mode and 817 W in the H-mode).

However, as can be seen from Fig. 8, B_ϕ component undergoes the most significant changes. In the E-mode, this is a purely linear signal with a sharp dip in the vicinity of $r=8$ cm. After transition to the H-regime, the strong second harmonic signal, with the amplitude four-fold higher than that of the fundamental harmonics, is generated. The B_ϕ component in the electromagnetic mode peaks at $r \sim 6$ cm. We note that a similar result has been observed in a higher-frequency ICP discharge.[12] The azimuthal rf magnetic field

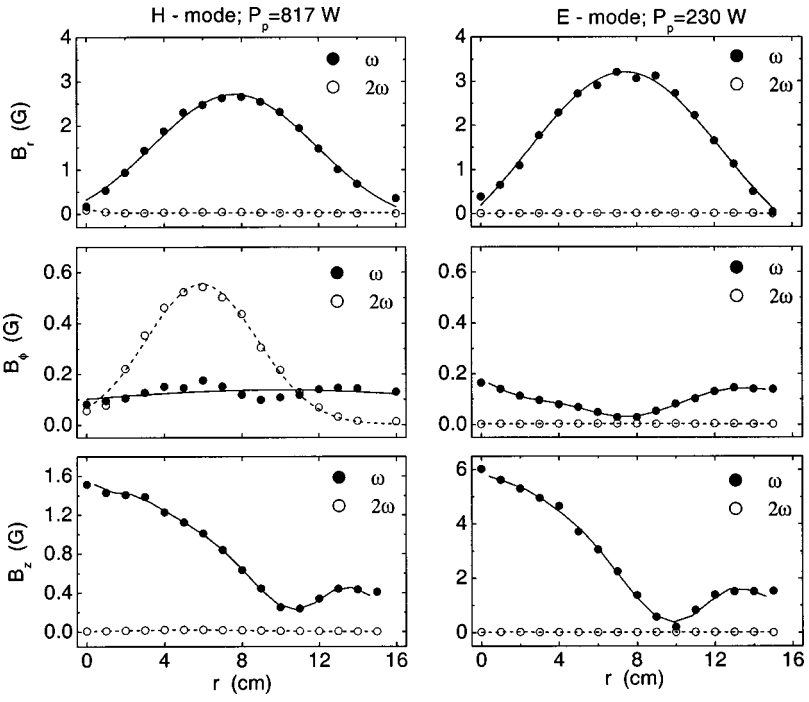

FIG. 8. Radial profiles of the amplitudes of B-field in the H- and E-mode measured at the mid-plane for a 51 mTorr Ar discharge showing the generation of a strong second harmonics of B_ϕ.

is presumably generated by the second harmonic poloidal ($r-z$ plane) current driven by the nonlinear Lorentz force arising as a result of action of $B_r(\omega)$ and $B_z(\omega)$ magnetic fields on the azimuthal rf current $j_\phi(\omega)$.

V. APPLICATIONS OF THE LF ICP SOURCE

In this section, we demonstrate the usefulness of the LF ICP source for the plasma enhanced nitrogen ion implantation and diffusion into the stainless steel and chemical vapor deposition of the DLC films.

It should be noted that depending on the process, either one of the two distinctive operation regimes can be used, which implies very high flexibility of the plasma source for certain applications. For instance, for rapid steel nitriding, the high-density H-mode appears to be preferable, while the diamond-like carbon films can be deposited in either one of the E or H regimes with different deposition rates.

A. Plasma enhanced nitriding of stainless steel

The AISI 304 stainless steel substrates have been used to study the nitrogen ion implantation and diffusion into a surface layer. The H-mode plasma has been generated in argon and nitrogen gas mixtures. An additional inlet of hydrogen allowed nitriding rates to be controlled. The substrates were negatively biased with respect to the plasma. The nitriding rates and morphology analysis have been performed with an inverted metallographic microscope. The surface hardness and tribological properties have been analyzed by means of the Vickers microhardness and wear tests. The elemental composition of the nitrided layer has been studied using the Energy Dispersive x-ray Analysis (EDXA).

The substrate temperature appears to be a key parameter of the nitriding process. The drawback of many conventional technologies is that relatively high nitriding rates are achieved with substrate temperatures, well above 500 °C. However, such temperatures adversely affect the corrosion performance of stainless steels owing to the precipitation of CrN, which removes chromium from a solid solution. In this experiment, the process has been performed at lower ($\sim$330 °C) steady-state temperatures achievable using an external heater control system.

Figure 9 displays the dependence of the Vickers hardness value on the substrate temperature, measured with a 100 g load at the nitriding depth of 25 μm. It is seen that very high values of hardness ($\sim$1300 Hv) can be achieved at a temperature of 330 °C, which is much lower than the usual substrate temperatures.

Figure 10(a) shows the hardness profile against the depth measured along the cross-section of the nitrided layer. The sample has been treated for 2 hours at the substrate temperature of 395 °C and the bias potential of 200 V. It is seen that 2 hours of plasma processing result in the 7-fold increase in the hardness value. The latter decreases slowly as one moves away from the top surface and eventually reaches the hardness of the steel matrix (185 Hv). The result implies that the nitrogen ion implantation/diffusion into the steel in the LF ICP source is a really very fast process. Indeed, the 2-hour treatment yields approximately 80 μm deep nitrided layers

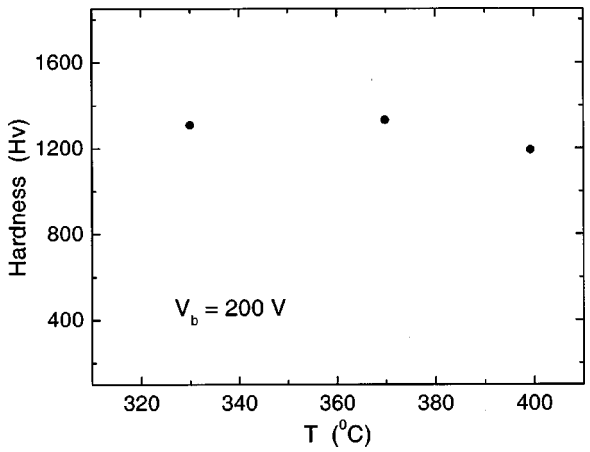

FIG. 9. Dependence of the micro-hardness on the substrate temperature *T*.

(Fig. 10). Dramatic enhancement of the steel hardness also results in $\sim$10 times improved wear resistance, which is evidenced by the ball-on-disk tribological wear tests.

Furthermore, it is found that distribution of the content of chromium remains constant over the entire substrate/nitrided layer whereas the nitrogen content gradually decreases in the nitrided layer and quickly drops near the boundary [Fig. 10(b)]. Hence, the problem of chromium depletion affecting the steel corrosion properties has been significantly minimized.

To demonstrate the uniformity of the nitrogen implantation/diffusion depth, a large, 22 cm diagonal AISI304 plate was placed on a modified substrate holder. To

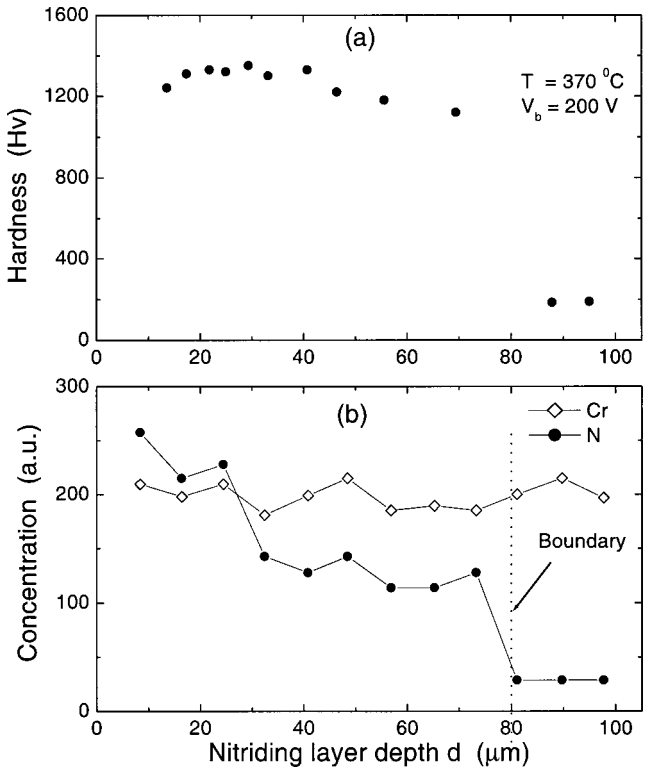

FIG. 10. The hardness profile versus the depth measured along the cross section (a) and the elemental distribution of chromium and nitrogen over the nitrided layer (b).

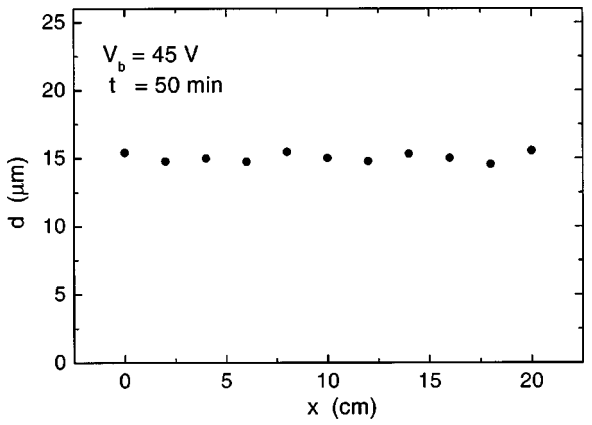

FIG. 11. Nitriding depth versus position *x*.

avoid overheating of the dc power supply by the excess ion current drawn by the large substrate, the nitriding process was undertaken at a minimal bias voltage of 45 V for relatively short time (50 min). The nitriding depth profile (Fig. 11) reveals that the nitrided layer is indeed highly uniform. The averaged variation of the layer thickness does not exceed 7% across the entire sample.

B. PECVD of DLC films

Another example of the application of the LF ICP source is the PECVD synthesis of the hydrogenated diamond-like carbon (DLC) films. For DLC film deposition, polished Si(100) substrates have been placed in the discharge in the CH_4 (20 sccm) and Ar (2 sccm) gas mixture. The thickness and the surface roughness of the films have been measured with a surface profilometer. The hardness and Young's modulus were characterized by a nanoindenter, using the continuous stiffness option with the maximum load of 10 mN.

The deposited films appear to be smooth and mechanically hard. The surface roughness ranges from 0.1 nm to 0.6 nm, depending on the rf power. The bonding states of the film material were analyzed by the Raman spectroscopy, which reveals the two typical peaks at 1374 cm^{-1} (disordered, D band) and 1546 cm^{-1} (graphitic, G band) characteristic to hydrogenated diamond-like carbon.

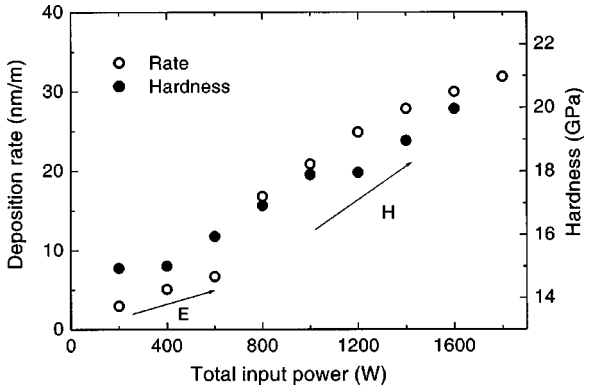

FIG. 12. The deposition rate and hardness of the DLC films as a function of the input rf power.

Figure 12 shows the film deposition rate and hardness as a function of the rf input power (at the bias voltage of 200 V). It is found that the deposition rate of the DLC film increases with rf power. In the low-power electrostatic regime, the film deposition rate is typically below 7.5 nm/min. Varying the rf power from 700 W to 1200 W, a substantial, from 10 nm/min to 35 nm/min, increase in the film deposition rate is clearly seen. Furthermore, the deposition process has been enhanced most noticeably in the power range of 700–800 W. The subsequent mechanical hardness tests reveal the improvement of the DLC film hardness from 15 to 21 GPa in the same range of input powers.

VI. DISCUSSION

We now discuss the features and implications of the low-frequency operation of the inductively coupled plasma source. First, operating in the two (E and H) regimes, the latter simultaneously embodies the asymmetric capacitive and flat spiral coil inductive plasma sources. Depending on a specific problem, the operation regime can be selected accordingly. For instance, the deposition rates and mechanical properties of the DLC films grown in the E and H discharge regimes appear to be different.

In the electromagnetic mode, the LF ICPs feature uniform, large-area, high-density plasmas with low sheath potentials near the substrate surface, independent control of the plasma density and the ion energy, high power transfer efficiency, low circuit loss and easy handling, and stable operation in a wide range of filling gas pressures. We need to stress that high-density, uniform plasmas is generated *without* any external magnetic confinement. This feature is highly desirable for low damage, large wafer semiconductor processing.[1,2]

In the electrostatic discharge mode, lower-density plasmas, with higher electron temperatures and plasma potentials are produced. We note that the ICP feature excellent uniformity of the electron/ion number density through the entire discharge cross-section and volume in the H-regime, and high cross-sectional uniformity in the E-mode.

The low-frequency operation offers several practical advantages including low skin-effect related circuit loss, easy control of the matching unit, high power transfer efficiency, easy diagnostics, and low voltage across the coil. The equivalent circuit analysis[14] shows that the capacitive rf field is too weak to cause any significant window sputtering. Furthermore, lowering of the operating frequency enables one to make the rf wavelength much longer than the coil length and eliminate the standing-wave effects peculiar to 13.56 MHz ICPs. This provides a practical solution for up-scaling of the ICP reactors without affecting the uniformity of electron and ion number densities.[5,20]

Another important feature of the LF ICP discharge is the wide range of operating pressures, which is very promising for multifunctional semiconductor processing. Indeed, the low pressure regime is favorable for deep-micron etching whereas high pressure is ideal for photo-resist striping.[1]

The experimental studies of plasma parameters and optical emission manifest that the nonlinear hysteresis effects

are inseparably associated with the mode jumps in LF ICPs. The reasons leading for hysteresis are still unclear and are the subject of ongoing investigations.[21] However, this phenomenon, alongside with generation of strong second harmonic signals, favors the implication that the entire behavior of the low-frequency discharge is strongly nonlinear. Physically, the plasma nonlinearities are stronger at lower frequencies.[18] Thus, the amplitudes of the nonlinear Lorentz force appear to be inversely proportional to the rf. Hence, the nonlinear interaction of B_r, B_z with the azimuthal rf current j_ϕ, leading to generation of strongly nonlinear poloidal currents is stronger at lower frequencies.

The other argument that confirms the strength of nonlinear effects in the discharge is the observed discrepancy of the measured highly uniform plasma density profiles with those obtained from conventional linear diffusion models.[17] One can presume that this could be the result of the ponderomotive force action, as well as other possible nonlinear effects. The adequate theoretical models for the above nonlinear phenomena still expect their realization. The fact that the amplitude of the second harmonics of B_ϕ appears of the same order as that of $B_{z,r}$ indicates that the conventional weakly nonlinear models can hardly be invoked for explanation, and the strongly nonlinear approaches have to be used instead.

It should be emphasized that the outstanding uniformity of the nitrided layer mirrors the electron density profiles (Sec. III). Thus, it is reasonable to assume that high and uniform plasma density is responsible for the rapid and uniform ion implantation/diffusion process. We note, however, that the classical diffusion solution does not adequately describe the dynamics of the rapid LF ICP nitriding process and needs substantial modification.[19]

We have demonstrated that the plasma density is a key factor in the deposition rate of the DLC films. In fact, the noticeable enhancement of the DLC film deposition process can be attributed to the E to H mode transition, which is accompanied by a great increment in the plasma density.

Another interesting advantage of the LF ICPs that go beyond the scope of this paper, include electron energy distribution functions (EEDF) with strong high energy tails (bi-Maxwellian EEDF) in the H-mode,[22] and bi-modal ion fluxes in the electrostatic regime.[23] Both features appear to be incredibly advantageous for control of the composition of active species in plasma chemistry.

VII. CONCLUSION

In this paper, we have studied the performance of the 500 kHz planar-coil inductively coupled plasma source. The global electrical characteristics of the discharge, distributions of the induced electromagnetic fields, plasma density, potential, electron temperature, and the optical emission spectra have been investigated. The processes of E-↔H-mode transitions have been verified. Several indisputable advantages of the low-frequency inductively coupled plasma source, such as very high plasma density, excellent uniformity over large areas, low electron temperature and a moderate plasma potential, absence of the Faraday shield or multipole magnetic confinement, low circuit loss, easy up-scaling, and easy operation, have been shown. We have also demonstrated that the LF ICP source is very efficient for plasma-enhanced nitriding of solid materials and PECVD thin film deposition. These results imply very attractive prospects for industrial applications of the planar-coil LF ICP source.

ACKNOWLEDGMENTS

We acknowledge the contribution of the members of the Plasma Processing Laboratory and fruitful discussions with S. Lee, R. Storer, Z. Sun, I. M. El-Fayoumi, M. Tuszewski, and H. Sugai.

K. N. O. thanks the Japan Society for the Promotion of Science for financial support. E. L. T. acknowledges the financial support of the NTU research Scholarship. This work was supported by AcRF Grants No. RG19/97, No. AcRF SX 19/97, and AcRF No. SX 4/99, and the Australian Research Council.

[1] *Plasma Etching: An Introduction*, edited by D. M. Manos and D. L. Flamm (Academic, New York, 1989).
[2] *Plasma–Surface Interactions and Processing of Materials*, edited by O. Auciello *et al.* (Kluwer Academic, Boston, 1990).
[3] M. A. Lieberman and A. J. Lichtenberg, *Principles of Plasma Discharges and Materials Processing* (Wiley, New York, 1994).
[4] J. Hopwood, Plasma Sources Sci. Technol. **1**, 109 (1992); J. H. Keller, *ibid.* **5**, 166 (1996); Plasma Phys. Controlled Fusion **39**, A437 (1997).
[5] M. Tsuzewski, Phys. Plasmas **5**, 1198 (1998); IEEE Trans. Plasma Sci. **27**, 68 (1999).
[6] H. Nakagawa, S. Morishita, S. Noda, M. Okigawa, M. Inoue, M. Sekine, and K. Ito, J. Vac. Sci. Technol. A **17**, 1514 (1999).
[7] V. A. Godyak, R. B. Piejak, B. M. Alexandrovich, and V. I. Kolobov, Phys. Plasmas **6**, 1804 (1999).
[8] I. M. El-Fayoumi, I. R. Jones, and M. M. Turner, Plasma Sources Sci. Technol. **7**, 3082 (1998).
[9] U. Kortshagen, N. D. Gibson, and J. E. Lawler, J. Phys. D **29**, 1224 (1996).
[10] K. Suzuki, K. Nakamura, H. Ohkubo, and H. Sugai, Plasma Sources Sci. Technol. **7**, 13 (1998).
[11] G. Cunge, B. Crowley, D. Vender, and M. M. Turner, Plasma Sources Sci. Technol. **8**, 576 (1999).
[12] V. A. Godyak, R. B. Piejak, and B. M. Alexandrovich, Phys. Plasmas **6**, 1804 (1999).
[13] R. B. Piejak and V. A. Godyak, Appl. Phys. Lett. **76**, 2188 (2000).
[14] I. M. El-Fayoumi and I. R. Jones, Plasma Sources Sci. Technol. **7**, 162 (1998); **7**, 179 (1998).
[15] K. N. Ostrikov, S. Xu, and M. Y. Yu, J. Appl. Phys. **88**, 2268 (2000).
[16] K.N. Ostrikov, S. Xu, and S. Lee, Phys. Scr. **62**, 189 (2000).
[17] S. Xu, K. N. Ostrikov, W. Luo, and S. Lee, J. Vac. Sci. Technol. A **18**, 2185 (2000).
[18] F. F. Chen, *Introduction to Plasma Physics and Controlled Fusion* (Plenum, New York, 1984).
[19] C. Chakrabarty, Ph.D. thesis, The Flinders University of South Australia, 1996.
[20] Y. Wu and M. A. Lieberman, Appl. Phys. Lett. **72**, 777 (1998).
[21] M. M. Turner and M. A. Lieberman, Plasma Sources Sci. Technol. **8**, 313 (1999).
[22] C. W. Chung, S. H. Seo, and H. Y. Chang, Phys. Plasmas **7**, 3584 (2000).
[23] E. A. Eidelberg and E. S. Aydil, J. Appl. Phys. **86**, 4799 (1999).